

Activation of CCR5 by Chemokines Involves an Aromatic Cluster between Transmembrane Helices 2 and 3*

Received for publication, June 8, 2002, and in revised form, October 24, 2002
Published, JBC Papers in Press, October 30, 2002, DOI 10.1074/jbc.M205685200

Cédric Govaerts^{†§¶}, Antoine Bondue^{†¶}, Jean-Yves Springael[‡], Mireia Olivella^{||}, Xavier Deupi^{||}, Emmanuel Le Poul^{**}, Shoshana J. Wodak^{‡‡}, Marc Parmentier^{‡§§}, Leonardo Pardo^{||}, and Cédric Blanpain[‡]

From the [‡]Institut de Recherche Interdisciplinaire en Biologie Humaine et Nucléaire, Université Libre de Bruxelles, Campus Erasme, 808 route de Lennik, B-1070 Bruxelles, Belgium, ^{||}Laboratori de Medicina Computacional, Unitat de Bioestadística, Facultat de Medicina, Universitat Autònoma de Barcelona, 08193 Bellaterra, Spain, ^{**}Euroscreen s.a., B-1070 Brussels, Belgium, and the ^{‡‡}Service de Conformation des Macromolécules Biologiques, Université Libre de Bruxelles, CP 160/16, Avenue F. Roosevelt, 1050 Bruxelles, Belgium

CCR5 is a G protein-coupled receptor responding to four natural agonists, the chemokines RANTES (regulated on activation normal T cell expressed and secreted), macrophage inflammatory protein (MIP)-1 α , MIP-1 β , and monocyte chemoattractant protein (MCP)-2, and is the main co-receptor for the macrophage-tropic human immunodeficiency virus strains. We have previously identified a structural motif in the second transmembrane helix of CCR5, which plays a crucial role in the mechanism of receptor activation. We now report the specific role of aromatic residues in helices 2 and 3 of CCR5 in this mechanism. Using site-directed mutagenesis and molecular modeling in a combined approach, we demonstrate that a cluster of aromatic residues at the extracellular border of these two helices are involved in chemokine-induced activation. These aromatic residues are involved in interhelical interactions that are key for the conformation of the helices and govern the functional response to chemokines in a ligand-specific manner. We therefore suggest that transmembrane helices 2 and 3 contain important structural elements for the activation mechanism of chemokine receptors, and possibly other related receptors as well.

Chemokine receptors have been dragging more and more attention since the cloning of the first member of the family a

* This work was supported by the Actions de Recherche Concertées of the Communauté Française de Belgique, the French Agence Nationale de Recherche sur le SIDA, the Centre de Recherche Inter-universitaire en Vaccinologie, the Belgian Programme on Interuniversity Poles of Attraction initiated by the Belgian State, Prime Minister's Office, Science Policy Programming, the BIOMED and BIOTECH programs of the European Community (Grants BIO4-CT98-0543 and BMH4-CT98-2343), the Fonds de la Recherche Scientifique Médicale of Belgium, Télévie, and the Fondation Médicale Reine Elisabeth (to M. P.). This work was also supported in part by Comisión Interministerial de Ciencia y Tecnología (Spain) Grant SAF2002-01509, a grant from Fundació La Marató TV3, and Improving Human Potential of the European Community Grant HPRI-CT-1999-00071. Computer facilities were provided by the Centre de Computació i Comunicacions de Catalunya. The costs of publication of this article were defrayed in part by the payment of page charges. This article must therefore be hereby marked "advertisement" in accordance with 18 U.S.C. Section 1734 solely to indicate this fact.

§ Current address: Dept. of Cellular and Molecular Pharmacology, University of California, San Francisco, San Francisco, CA 94143.

¶ These two authors contributed equally to this work.

§§ To whom correspondence should be addressed: IRIBHN, Université Libre de Bruxelles, Campus Erasme, 808 route de Lennik, B-1070 Bruxelles, Belgium. Tel.: 32-2-555-41-71; Fax: 32-2-555-46-55; E-mail: mparment@ulb.ac.be.

decade ago. Not only are chemokines and their receptors now considered as the main organizers of leukocyte trafficking, they have also been associated to an ever increasing number of physiopathological disorders (for review, see Refs. 1 and 2). In particular, some chemokine receptors are used by the human immunodeficiency virus (HIV)¹ as coreceptors (in addition to CD4) to infect target cells (reviewed in Ref. 3). Among these, CCR5 has been shown to be essential for HIV pathogenesis, as individuals homozygous for the CCR5 Δ 32 mutation, which results in the synthesis of a non-functional receptor, are highly (although not fully) resistant to HIV infection. Chemokine receptors belong to the rhodopsin-like family (family A) of G protein-coupled receptors (GPCR). CCR5 binds and responds to four natural chemokines, RANTES, MIP-1 α , MIP-1 β , and MCP-2, with nanomolar affinities (4).

Our current understanding of the activation mechanisms of GPCRs is rapidly evolving, thanks to the availability of the crystal structure of the inactive state of one of its members, rhodopsin, and to the growing amount of biochemical and physicochemical data that can help in identifying the key aspects of this process (for review, see Refs. 5 and 6). It is now well accepted that the transition from inactive to active states requires the reorganization of the transmembrane bundle made of seven imperfect α -helices. In the rhodopsin-like family, motions of transmembrane helix 3 (TM3) and TM6 during the activation process have been identified (7–9). Rigid-body movements have also been proposed for TM5 and TM7 (10, 11). Most of these conformational changes have been observed in a diverse set of receptors (mainly rhodopsin and the β_2 -adrenergic receptor), and it is believed that they constitute a common conformational path in the activation process, ultimately leading to the release of GDP from the bound G protein and its exchange for GTP.

A striking feature within the rhodopsin-like GPCR family is that, despite a strong sequence conservation of the transmembrane helices, there is a wide structural diversity among extracellular ligands, ranging from small neurotransmitters to large glycoproteins. The structural adaptation of a receptor to its

¹ The abbreviations used are: HIV, human immunodeficiency virus; GPCR, G protein-coupled receptor; TM, transmembrane helix; ECL, extracellular loop; ICL, intracellular loop; MD, molecular dynamics; MIP, macrophage inflammatory protein; MCP, monocyte chemoattractant protein; wt, wild-type; RANTES, regulated on activation normal T cell expressed and secreted; PDB, Protein Data Bank; GTP γ S, guanosine 5'-3-O-(thio)triphosphate; CHO, Chinese hamster ovary; MAP, mitogen-activated protein; DMEM, Dulbecco's modified Eagle's medium; Tricine, N-[2-hydroxy-1,1-bis(hydroxymethyl)ethyl]glycine.

cognate ligand is expected to involve, in most cases, sequence specificity in the extracellular domains (for which sequence conservation is much lower across the family), but also in the transmembrane region, which holds the binding pocket of small ligands (for reviews, see Refs. 6 and 12). Therefore, each receptor must have evolved specific structural characteristics to link the specific recognition of its cognate ligand to what is believed to constitute a common activation process (e.g. motion of TM6). Thus, for each receptor subfamily, specific structural features needed for the activation by agonists are expected to be found.

In the case of chemokine receptors, we have recently identified a structural motif in TM2, which is central for chemokine-induced activation (13). This motif, which consists of a proline preceded by a threonine two residues ahead (TXP), is found only in chemokine receptors and a few related peptide receptors. Our study indicated that the extracellular part of TM2, whose conformation is governed by the TXP motif, is clearly involved in the activation process, as specific mutations of the motif led to unaffected chemokine binding but strong impairment of receptor activation (13). Moreover, modeling studies performed on this region suggested that, because of the action of the proline, the extracellular part of TM2 would strongly interact with TM3. This organization is structurally different from that of bovine rhodopsin, in which a TM2-TM1 interaction is found.

As a follow-up of these observations, we have now investigated the possible role of the TM2-TM3 interface in the activation process of chemokine receptors. A sequence alignment of chemokine receptors (Fig. 1) reveals that the extracellular parts of TM2 and TM3 contain many aromatic residues. Within the rhodopsin template, these residues are located at relatively short distances, suggesting that they might form an aromatic cluster within the three-dimensional structure of the receptors. Aromatic residues have been proposed to be involved in the activation mechanism in various GPCRs (14–22). Among other examples, a role was attributed to such residues in the ligand selectivity and ligand-induced activation of the D2 and D4 dopamine receptors (20, 23). The high density of aromatic residues at the top of TM2 and TM3 in chemokine receptors suggested that aromatic side chains could mediate interactions between these helices.

In the present study, we have mutated the aromatic residues of CCR5 TM2 and TM3 into their CCR2 counterparts, either individually or in combination, and the mutants were tested for cell-surface expression, receptor conformation, ligand binding, and functional response. Molecular modeling of the transmembrane region of CCR5 has been performed, providing a structural framework to interpret these data. Integration of the experimental and molecular modeling data indicates that aromatic residues at the TM2-TM3 interface are crucial to the mechanism of receptor activation and suggests that this aromatic cluster plays a key role in the conformational changes of CCR5, leading from ligand recognition to receptor activation.

EXPERIMENTAL PROCEDURES

Numbering Scheme of GPCRs—In this work, we use a general numbering scheme to identify residues in the transmembrane segments of different receptors (24). Each residue is numbered according to the helix (1 through 7) in which it is located and to the position relative to the most conserved residue in that helix, arbitrarily assigned to 50. For instance Pro-2.58 is the proline in the transmembrane helix 2 (TM2), eight residues following the highly conserved aspartic acid Asp-2.50. For the sake of clarity, generalized numbers are italicized. When both numbers are given, the general numbering is put as superscript.

Survey of Transmembrane Helices Containing a FWXXY Motif in Known Membrane Protein Structures—We surveyed the atomic coordinates of the membrane proteins bacteriorhodopsin (PDB access number

1c3w, 1.55 Å resolution), aa3 (1occ, 2.8 Å) and ba3 (1ehk, 2.4 Å) cytochrome *c* oxidases, photosynthetic reaction center (1prc, 2.3 Å), potassium channel (1bl8, 3.2 Å), mechanosensitive ion channel (1msl, 3.5 Å), rhodopsin (1f88, 2.8 Å), halorhodopsin (1el2, 1.8 Å), sensory rhodopsin (1h68, 2.1 Å), light harvesting complex (1lgh, 2.4 Å), photosystem I (1jbo, 2.5 Å), AQP1 (1hwo, 3.7 Å) and GlpF (1fx8, 2.2 Å) channels, P-type ATPase (1eul, 2.6 Å), and fumarate reductase respiratory complex (1qla, 2.2 Å) for α -helical segments featuring the FWXXY motif.

Molecular Dynamics Simulations of Transmembrane Helices—The model peptides Ace-Ala₁₁-Thr-Ala-Pro-Ala₁₁-Nme and Ace-Ala₇-Thr-Gly-Ala₄-Gly-Ala₂-Ser-Gly-Ala₁₅-Nme were built in the standard α -helical conformation ($\phi, \psi = -58^\circ, -47^\circ$). The amino acid side chains of Ser and Thr were set to the *g+* conformation. Molecular dynamics simulations of these model peptides aim to explore the conformation of TM2 in CCR5 triggered by the Thr-2.56-X-Pro-2.58 motif and TM3 triggered by the presence of Thr-3.29, Gly-3.30, Gly-3.35, Ser-3.38, and Gly-3.39. A similar approach was recently used to model the conformation of TM3 in the 5HT_{1A} serotonin receptor (25). Ser and Thr residues induce a small bending angle in TM because of the additional hydrogen bond formed between the O γ atom of Ser or Thr and the *i*-3 or *i*-4 peptide carbonyl oxygen (26). Moreover, the additional flexibility provided by the adjacent Pro (because of the absence of the hydrogen bond with the carbonyl oxygen in the preceding turn of the helix) or Gly (because of the lack of the side chain) reinforces this effect. The obtained structures were placed in a rectangular box containing methane molecules to mimic the hydrophobic environment of the TM bundle. The peptide-methane systems were subjected to 500 iterations of energy minimization and then heated to 300 K in 15 ps. This was followed by an equilibration period (15–500 ps) and a production run (500–1500 ps) at constant volume using the particle mesh Ewald method to evaluate electrostatic interactions. Structures were collected for analysis every 10 ps during the production run (100 structures/simulation). To obtain a rough idea of the possible consequences that the presence of these residues in TM2 and TM3 might have on the structure of the receptor, we performed a molecular modeling exercise using the three-dimensional structure of rhodopsin as the template. The backbone of one helical turn preceding the highly conserved Asp-2.50 in TM2 and (D/E)R3.50Y motif in TM3 superimposed the helix bundle of rhodopsin with the computed structures.

Molecular Dynamics Simulations of the CCR5 Receptor and Mutant Receptors—The three-dimensional model of transmembrane helices 1 and 4–7 of CCR5 was constructed by computer-aided model building techniques from the transmembrane domain of bovine rhodopsin, as determined by Palczewski *et al.* (27). The following conserved residues were employed in the alignment of rhodopsin and human CCR5 transmembrane sequences: Asn-55 (55 being the residue number in the 1F88 PDB file of rhodopsin) and Asn-48^{1.50} (48 is the residue number in the CCR5 sequence, 1.50 in the standardized numbering); Trp-161 and Trp-153^{4.50}; Pro-215 and Pro-206^{5.50}; Pro-267 and Pro-250^{6.50}; and Pro-303 and Pro-294^{7.50}. Representative structures of transmembrane helices 2 and 3, selected by automatically clustering the geometries obtained during the molecular dynamics trajectories into conformationally related subfamilies with the program NMRCLUST (28), were included into the model (see “Molecular Dynamics Simulations of Transmembrane Helices” above). SCWRL-2.1 was employed to add the side chains of the non-conserved residues based on a backbone-dependent rotamer library (29). All ionizable residues in the helices were considered uncharged with the exception of Asp-2.40, Asp-2.50, Asp-3.49, Arg-3.50, Lys-5.50, Arg-6.30, Arg-6.32, and Glu-7.39. To relieve residual strain resulting from suboptimal positioning of the side chains and the TM2-TM3 interface at the extracellular part, this resulting initial structure was placed in a rectangular box containing methane molecules, energy-minimized (500 steps), heated (from 0 to 300 K in 15 ps), and equilibrated (from 15 to 100 ps). During these processes, the C α atoms were kept fixed at their positions in the rhodopsin crystal structure, with the exception of the residues forming the TM2-TM3 interface (from 2.58 to 3.29). The optimized TM2-TM3 interface accomplishes: (i) the distance between the top (C terminus) of TM2 and the top (N terminus) of TM3 is in the 10–11-Å range to allow the first extracellular loop (ECL1) of 4 residues to be shaped; (ii) Phe-85^{2.59} interacts with Leu-104^{3.28} and Tyr-89^{2.63} interacts with Thr-99^{3.23}, in a similar manner to the cytochrome *c* oxidase structure of helices III and VII in subunit III (see “Results”); and (iii) there are not steric clashes between helices. The interactions of the side chain of Leu-104^{3.28} with the side chains of Phe-85^{2.59} and Trp-86^{2.60} were further characterized by *ab initio* quantum mechanical calculations at the MP2/6–31G* level of theory, which is capable of describing the proposed C-H \cdots π interactions (30).

Molecular models of the helix bundles for the mutant receptors containing the F85^{2.59}L, L104^{3.28}F, F85^{2.59}L/L104^{3.28}F, F109^{3.33}H, F112^{3.36}Y, and F109^{3.33}H/F112^{3.36}Y substitutions were constructed from the previously obtained structure of CCR5, by changing the atoms implicated in the amino acid substitutions by interactive computer graphics. Subsequently, wild-type and mutant receptors were placed in a rectangular box (~71 Å × 60 Å × 50 Å in size) containing methane molecules (~2850 molecules in addition to the transmembrane domain) to mimic the hydrophobic environment of the transmembrane helices. The density of 0.4–0.5 g cm⁻³ of the methane box is approximately half of the density observed in the hydrophobic core of the membrane. This is a result of the different equilibrium distance between carbons in the methane box and in the polycarbon chain of the lipid. However, it has been shown that this procedure reproduces several important structural characteristics of membrane embedded proteins (31). The receptor-methane systems were subjected to 500 iterations of energy minimization and then heated to 300 K in 15 ps. This was followed by an equilibration period (15–100 ps) and a production run (100–250 ps) at constant volume using the particle mesh Ewald method to evaluate electrostatic interactions (32). Structures were collected for analysis every 10 ps during the production run (15 structures per simulation). The molecular dynamics simulations were run with the Sander module of AMBER 5 (33), the all-atom force field (34), SHAKE bond constraints in all bonds, a 2-fs integration time step, and constant temperature of 300 K coupled to a heat bath.

CCR5 Mutants—Plasmids encoding the CCR5 mutants studied here were constructed by site-directed mutagenesis using the QuikChange method (Stratagene). Following sequencing of the constructs, the mutated coding sequences were subcloned into the bicistronic expression vector pEFIN3 as previously described for generation of stable cell lines (35). All constructs were verified by sequencing prior to transfection.

Expression of Mutant Receptors in CHO-K1 Cells—CHO-K1 cells were cultured in Ham's F-12 medium supplemented with 10% fetal calf serum (Invitrogen), 100 units/ml penicillin, and 100 µg/ml streptomycin (Invitrogen). Constructs encoding wild-type or mutant CCR5 in the pEFIN3 bicistronic vector were transfected using FuGENE 6 (Roche Molecular Biochemicals) in a CHO-K1 cell line expressing an apoaequorin variant targeted to mitochondria (36). Selection of transfected cells was made for 14 days with 400 µg/ml G418 (Invitrogen) and 250 µg/ml zeocin (Invitrogen, for maintenance of the apoaequorin encoding plasmid), and the population of mixed cell clones expressing wild-type or mutant receptors was used for binding and functional studies. Cell surface expression of the receptor variants was measured by flow cytometry using monoclonal antibodies recognizing different CCR5 epitopes: 2D7 (phycoerythrin-conjugated, PharMingen), MC-1, MC-4, MC-5, and MC-6 (kindly provided by Mathias Mack, Munich, Germany). Unlabeled monoclonal antibodies were detected by an anti-mouse IgG phycoerythrin-coupled secondary antibody (Sigma).

Binding Assays—CHO-K1 cells expressing wild-type or mutant CCR5 were collected from plates with Ca²⁺/Mg²⁺-free phosphate-buffered saline supplemented with 5 mM EDTA, gently pelleted for 2 min at 1000 × g, and resuspended in binding buffer (50 mM Hepes, pH 7.4, 1 mM CaCl₂, 5 mM MgCl₂, 0.5% bovine serum albumin). Competition binding assays were performed in Minisorb tubes (Nunc), with 40,000 cells in a final volume of 0.1 ml. The mixture contained 0.05 nM [¹²⁵I]-RANTES (2000 Ci/mmol, Amersham Biosciences) or 0.1 nM [¹²⁵I]-MIP-1β as tracer, and variable concentrations of competitors (R&D Systems). Total binding was measured in the absence of competitor, and nonspecific binding was measured with a 100-fold excess of unlabelled ligand. Samples were incubated for 90 min at 27 °C, then bound tracer was separated by filtration through GF/B filters pre-soaked in 0.5% polyethyleneimine (Sigma) for [¹²⁵I]-RANTES or in 0.1% bovine serum albumin (Sigma) for [¹²⁵I]-MIP-1β. Filters were counted in a β-scintillation counter. Binding parameters were determined with the Prism software (GraphPad Software) using non-linear regression applied to a one site competition model.

Aequorin Assay—Functional response to chemokines was analyzed by measuring the luminescence of aequorin as described (37, 38). Cells were collected from plates with Ca²⁺/Mg²⁺-free DMEM supplemented with 5 mM EDTA. They were then pelleted for 2 min at 1000 × g, resuspended in DMEM at a density of 5 × 10⁶ cells/ml, and incubated for 2 h in the dark in the presence of 5 µM coelenterazine H (Molecular Probes). Cells were diluted 5-fold before use. Agonists in a volume of 50 µl DMEM were added to 50 µl of cell suspension (50,000 cells), and luminescence was measured for 30 s in a Berthold Luminometer.

GTPγS Binding Assay—The measurement of chemokine-stimulated GTPγS binding to membranes of cells expressing wt-CCR5 or the Y108A mutant were performed as described (39, 40). Briefly, mem-

branes (10 or 20 µg) from wt-CCR5 or Y108A cells were incubated for 15 min at room temperature in GTPγS binding buffer (20 mM Hepes, pH 7.4, 100 mM NaCl, 3 mM MgCl₂, 3 µM GDP, 10 µg/ml saponin) containing different concentrations of chemokines, in 96-well microplates (Basic FlashPlates, PerkinElmer Life Sciences). [³⁵S]GTPγS (0.1 nM, Amersham Biosciences) was added, microplates were shaken for 1 min and further incubated at 30 °C for 30 min. The incubation was stopped by centrifugation of the microplate for 10 min, at 800 × g and 4 °C, and aspiration of the supernatant. Microplates were counted in a TopCount (Packard, Downers, IL) for 1 min/well. Functional parameters were determined with the PRISM software (GraphPad Software) using non-linear regression applied to a sigmoidal dose-response model.

MAP Kinase Assay—Cells, serum-starved for 24 h, were collected and resuspended in serum-free DMEM. After 3 min of stimulation with various concentrations of RANTES and MCP-2, cells were collected by centrifugation and heated to 100 °C for 5 min in lysis buffer (100 mM Tris-HCl, pH 6.8, 4 mM EDTA, 4% SDS, 20% glycerol, and 0.02% β-mercaptoethanol). For Western blot analysis, solubilized proteins corresponding to ~5 × 10⁵ cells were loaded onto 10% SDS-polyacrylamide gels in a Tricine buffer system (41). After transfer to nitrocellulose membranes, proteins were probed with mouse anti-phospho-p42/p44 (1:1000) (Cell Signal) or rabbit anti-total p38 (1:2000) antibodies (Santa Cruz).

RESULTS

To investigate the possible role of aromatic residues at the TM2-TM3 interface in defining the structure and function of the CCR5 receptor, we have compared the amino acid sequences of CCR2 and CCR5 (Fig. 1B). These receptors are strongly related, sharing ~85% sequence identity within their TM helices. However, their extracellular domains are much more divergent, which certainly contributes to their strong selectivity toward their respective ligands (35). The TM2-TM3 aromatic cluster was found to be quite divergent between the two receptors. This could suggest that these positions are not important for the structure and/or function of the receptors and therefore highly tolerant to variability. Alternatively, these positions could be functionally important although specific to each receptor, and the various substitutions would be expected in this case to be correlated. To study the functional consequences of the differences at aromatic positions observed between CCR5 and CCR2 (Fig. 1B), we engineered CCR5 mutants in which aromatic residues were substituted by the corresponding amino acids in CCR2. The F85^{2.59}L and Y89^{2.63}S mutants affected TM2, L104^{3.28}F; F109^{3.33}H and F112^{3.36}Y involved TM3. We also combined these point mutations either within TM2 (F85L/Y89S double mutant), within TM3 (F109H/F112Y, L104F/F109H/F112Y), or across both helices (F85L/L104F, Y89S/L104F, F85L/Y89S/L104F).

Cell Surface Expression of the Mutant Receptors

We determined cell surface expression of the CCR5 mutants by fluorescence-activated cell sorting analysis, using five well characterized monoclonal antibodies (40, 42). The epitopes recognized by these monoclonal antibodies have been mapped to the N-terminal domain of the receptor (MC-5 and 3A9), the second extracellular loop (2D7), or a combination of extracellular domains (523 and MC6).

Fig. 2 illustrates the average surface expression of the different mutants following normalization to wild-type CCR5 expression level. The TM2 mutant F85L exhibited a moderate but significantly reduced expression, reaching ~50% of the wt signal. Although the Y89S mutant was well expressed, the combination of both substitutions (F85L/Y89S) led to a reduced expression similar to that of F85L. Interestingly, although the single mutation L104F (in TM3) did not affect cell surface expression, its combination with F85L restored to normal the low expression observed for F85L alone (mutant F85L/L104F). Strikingly, the triple mutant F85L/Y89S/L104F was not found at the cell surface, indicating that, although single and double

FIG. 1. Alignment of TM2 and TM3 sequences from chemokine receptors. A, alignment comprising TM2 and TM3 for the different chemokine receptors. The generalized numbering scheme (see “Experimental Procedures”) is used to label the alignment. Aromatic residues are highlighted in *bold characters*, whereas the TXP motif is *boxed*. The limits of the helices were defined as those observed for bovine rhodopsin (27). B, subset of the alignment focusing on the sequence differences between CCR5 and CCR2. Aromatic residues differing between the two receptors are in *bold* and marked by *arrows*. The CCR5 numbering for these positions is given above the sequence.

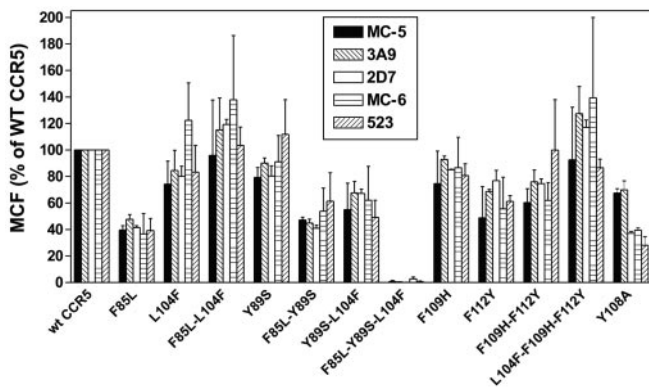
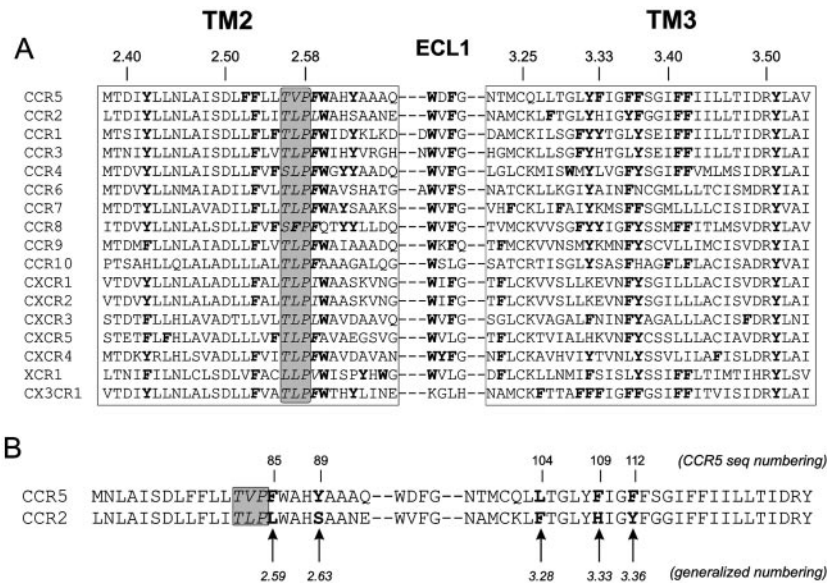


FIG. 2. Expression efficiency of the receptor mutants. Cell-surface expression of wt-CCR5 and the different mutants measured by fluorescence-activated cell sorting using five different monoclonal antibodies. The data are representative of three independent experiments. The 2D7 antibody recognizes a conformational epitope centered on ECL2, MC-6 and 523 recognize multidomain conformational epitopes, whereas MC-5 and 3A9 target epitopes located in the N-terminal domain of CCR5. Values represent the mean (error bars: S.E.) of the mean cell fluorescence obtained in three different experiments, normalized by the value obtained for CCR5 (100%) separately for each antibody.

mutants are expressed, the combination of all three substitutions is not tolerated. This mutant will therefore not be considered further in the following experimental settings. Mutants Y89S/L104F, F109H, F112Y, F109H/F112Y, and L104F/F109H/F112Y are all expressed above 50% of the wt signal with a rather uniform pattern of recognition by the different monoclonal antibodies, suggesting that these mutations do not alter the conformation of CCR5 extracellular domains.

Binding and Functional Properties of the Mutant Receptors

The functional consequences of the mutations and their combinations were characterized in terms of binding and intracellular responses, using the four natural agonists of CCR5: RANTES, MIP-1 α , MIP-1 β , and MCP-2. The binding affinities for the various ligands were determined by competition binding assays using 125 I-RANTES or 125 I-MIP-1 β as labeled tracer, whereas functional responses were monitored by using the aequorin-based assay as described previously (13). Representative binding curves are shown in Fig. 3, functional concentra-

tion-action curves are shown in Fig. 4, and the data are summarized in Table I.

We first focused on residues Phe-85, Tyr-89, and Leu-104, located at the extracellular ends of TM2 and TM3. The F85L mutant was clearly impaired both at the level of binding, and in its functional response to chemokines. Although binding of RANTES was almost unaffected, the apparent affinities for MIP-1 β and MCP-2 were significantly lower than those observed for wt-CCR5 (see Table I and Fig. 3), and MIP-1 α binding was undetectable. The functional responses of F85L were mild (Fig. 4) and grossly consistent with the binding data. The potency of RANTES was moderately affected on this mutant, but its efficacy was reduced by 4-fold; MIP-1 β and MCP-2 displayed a strong impairment of both their potencies and efficacies, whereas MIP-1 α was almost inactive. The phenotype of the L104F mutant was grossly similar in terms of functional responses (with slightly better efficacies) despite binding parameters much closer to the wild-type levels. Interestingly, the addition of the L104F substitution to the F85L mutant (F85L/L104F) allowed partial restoration of the function of this mutant. Indeed, on the double mutant, MIP-1 α was characterized by a binding affinity close to wt, and the functional response was significantly improved. The functional properties of MCP-2 appeared somewhat more affected by the double mutation, whereas RANTES and MIP-1 β showed similar behaviors on the double mutant and on both single mutants.

Mutating Y89S affected mildly the activity of RANTES and MIP-1 α (conserved potency, 2-fold reduction of E_{\max}) decreased moderately the E_{\max} and potency of MIP-1 β , but affected strongly the functional parameters of MCP-2, despite the normal affinity of this mutant in binding assays. Combining F85L and Y89S substitutions led to a severe impairment of functional responses, particularly for MIP-1 β and MCP-2 (no response), and to a lower extent for MIP-1 α , whereas RANTES was moderately affected. These effects appeared more than simply additive as compared with the single mutants. The Y89S/L104F mutant was well expressed at the cell surface, but no specific binding could be detected by competition binding assays, and this receptor was barely functional. Only RANTES could elicit a small signal at high concentrations, with a strongly reduced E_{\max} but a decent potency (Table I).

Modeling the TM2-TM3 Interface

The experimental data presented above demonstrate the importance of the TM2-TM3 aromatic cluster in the activation

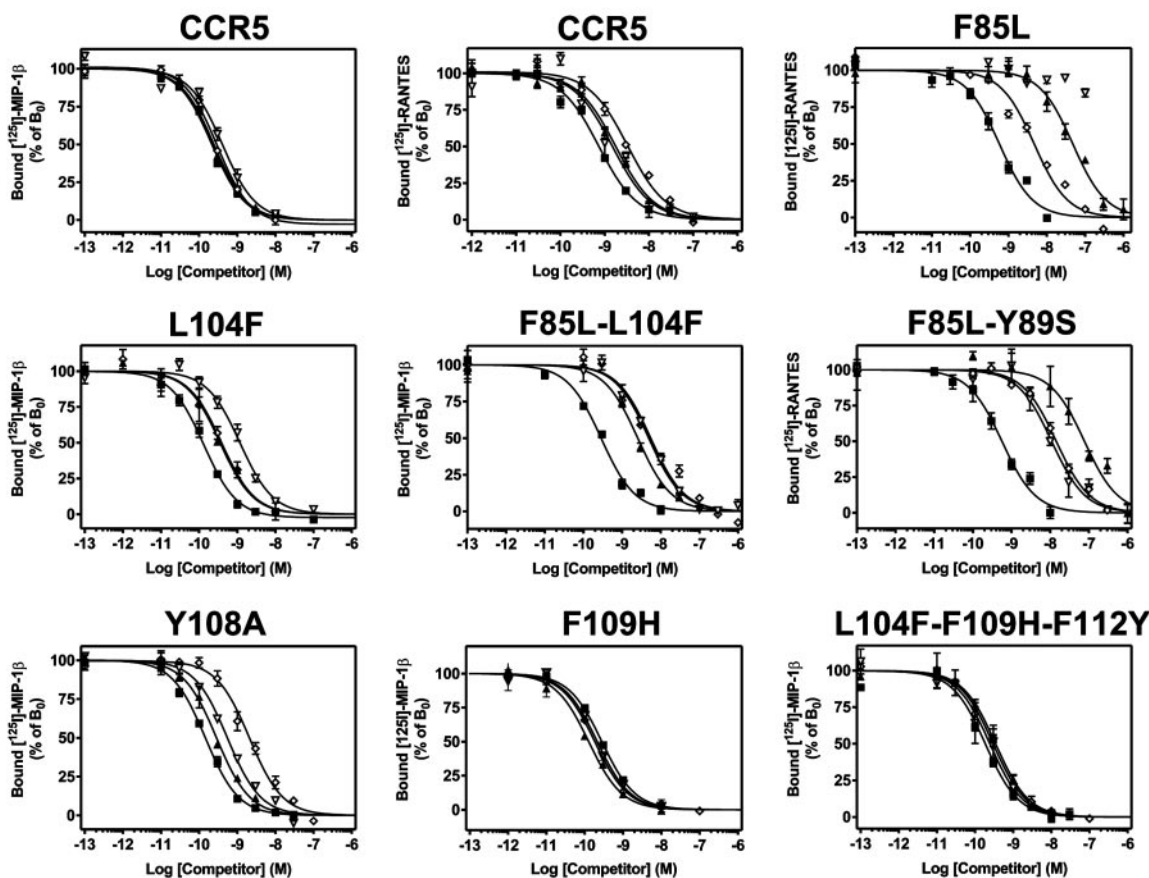


FIG. 3. **Binding properties of the wt and mutant receptors.** Competition binding assays on CHO-K1 cell lines expressing wt-CCR5 and the different mutants using ^{125}I -RANTES or ^{125}I -MIP-1 β as tracer. The data are representative of at least two experiments. Results were analyzed by the GraphPad Prism software, using a single-site model, and the data were normalized for nonspecific (0%) and specific binding in the absence of competitor (100%). All points were run in triplicate (error bars: S.E.). Unlabeled ligands are RANTES (■), MIP-1 β (▲), MIP-1 α (▼), and MCP-2 (◇).

of CCR5. The fact that adding the L104F substitution to the F85L background partly restores the impaired function of this mutant (cell-surface expression and binding) might suggest a direct interaction between the two residues involved. Moreover, Tyr-89 might contribute to this interaction, as mutating this residue, although well tolerated by itself, is highly disruptive in the context of F85L, Y89S, or F85L/Y89S. Fig. 6A shows the location of the side chains of these residues in a CCR5 model using strictly the rhodopsin crystal as a template (27). The orientation of these side chains toward the lipidic environment is in apparent contradiction with the hypothesis that these residues are important for the structure and the activation mechanism of CCR5.

We have, however, suggested previously that TM2 of CCR5 would adopt, in its outer half, a conformation that is different from that of bovine rhodopsin (13). In CCR5 and other chemokine receptors, the extracellular side of TM2 is predicted to be in close contact with TM3 (and not with TM1 as in rhodopsin) as a result of the structural action of a conserved Thr2.56-X-Pro2.58 motif (13). We now propose that this region of TM2 would be part of a structural and functional motif involving the neighboring part of TM3 (aromatic cluster and surrounding residues).

To provide a structural framework allowing to understand better the experimental data presented above, we adopted a modeling procedure (detailed under “Experimental Procedures”) based on the following scheme.

Independent Exploration of the Conformation of TM2 and TM3 by Molecular Dynamics Simulations—Fig. 6 (B and C) shows the computed structures of TM2 (green) and TM3 (yellow). The bending of TM2 toward TM3, in its outer half, is tolerated in the

context of the CCR5 helical bundle as the result of the relocation of TM3 toward TM5. It is important to note that these energetically available structures of TM2 and TM3 were obtained separately. Thus, the conformational spaces explored by these helices are the consequence of the amino acid sequence of TM2 and TM3 and not of steric hindrance between helices.

The TM2-TM3 Interface Was Further Optimized by MD Simulations of the Seven-helix Bundle in an Apolar Environment—Fig. 6 (D and E) shows the result of superimposing the representative structure of the MD simulation and the rhodopsin template. The specific residues in TM2 and TM3 of CCR5 generate structural differences in the extracellular part of the receptor, without modifying its more compact cytoplasmic surface.

Membrane Protein Data Base Search—Because stable structural motifs are likely to recur in proteins of known structure, we surveyed the data base of the structure of membrane proteins (see “Experimental Procedures”) for α -helix segments containing the aromatic cluster of TM2: the FWXXY motif. This motif is also found in subunit III of the bovine cytochrome *c* oxidase (PDB identification code 1occ), where transmembrane helix III of the enzyme interacts with the neighboring helix VII. Inspection of this motif in the cytochrome *c* oxidase structure reveals that the Phe-98 side chain in helix III interacts with Leu-252 residue in helix VII, and that the Tyr-102 side chain in helix III hydrogen bonds Ser-255 in helix VII. We propose a similar pattern to describe the interactions between TM2 and TM3 of CCR5; Phe-85 would interact with Leu-104, and Tyr-89 with Thr-99. It is important to note that Phe-85, Tyr-89, Thr-99, and Leu-104 are found specifically in CCR5, but not in CCR2, and contrib-

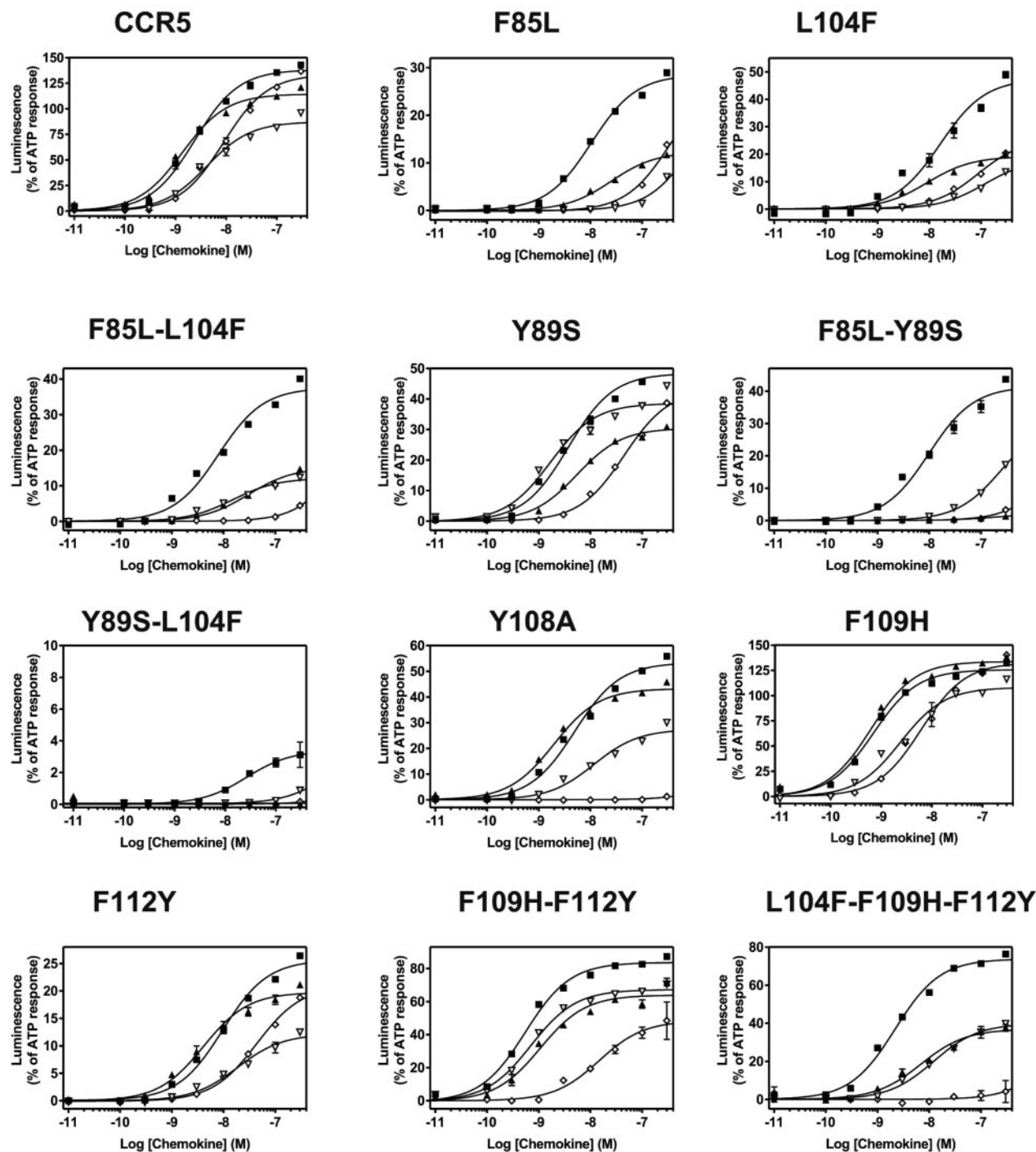


FIG. 4. **Activation of the different receptors by the four CCR5 agonists.** Functional response to RANTES (■), MIP-1 β (▲), MIP-1 α (▼), and MCP-2 (◇) of CHO-K1 cells expressing wt-CCR5 or the various mutants, using the aequorin assay. All points were run in triplicate (error bars: S.E.). The displayed curves represent a typical experiment out of at least three performed independently. Results were analyzed by nonlinear regression using the GraphPad Prism software. Data were normalized to maximal cell line stimulation by a saturating concentration of ATP. Note that the vertical scales of the graphs have been adapted to the maximal responses obtained for each line.

ute therefore to a CCR5-specific motif important for the receptor structure.

Fig. 7A shows a detailed view of the TM2-TM3 interface in the model resulting from MD simulation. In this model, Leu-104 is located in an aromatic pocket formed by the side chains of Phe-85 and Trp-86, and the electron-poor C-H hydrogens of L104 interact with the π electron-rich clouds of the aromatic rings. This type of C-H $\cdots\pi$ interaction plays a significant role in stabilizing local three-dimensional structures of proteins (43). Moreover, Phe-85 aromatic ring is located between Leu-

103 and Leu-104 side chains. Thus, there is a significant interaction between the aromatic residues (Phe-85 and Trp-86) in TM2 and the hydrophobic residues (Leu-103 and Leu-104) in TM3. In addition, the TM2-TM3 interface is stabilized by a hydrogen bond between Tyr-89 and Thr-99. To evaluate the magnitude of the TM2-TM3 interaction that might be attributed to the Phe-85 \cdots Leu-104 and Trp-86 \cdots Leu-104 interactions, we performed *ab initio* quantum mechanical calculations on minimal recognition models consisting of the functional groups of the intervening side chains (see

TABLE I
Binding and functional properties of wt-CCR5 and mutant receptors

The pIC₅₀ (−log M) values were obtained from competition binding experiments, using ¹²⁵I-RANTES or ¹²⁵I-MIP-1β as a tracer. Values represent the mean ± S.E. of at least two independent determinations. The pEC₅₀ (−log M) values were obtained from functional dose-response curves using the acquirin assay. Values represent the mean ± S.E. of at least three independent determinations. —, not done. NM, not measurable; no specific binding could be detected.

	RANTES				MIP-1β				MIP-1α				MCP-2			
	Binding		Function		Binding		Function		Binding		Function		Binding		Function	
	MIP-1β pIC ₅₀	RANTES pIC ₅₀	pEC ₅₀	E _{max}	MIP-1β pIC ₅₀	RANTES pIC ₅₀	pEC ₅₀	E _{max}	MIP-1β pIC ₅₀	RANTES pIC ₅₀	pEC ₅₀	E _{max}	MIP-1β pIC ₅₀	RANTES pIC ₅₀	pEC ₅₀	E _{max}
CCR5	9.64 ± 0.08	9.13 ± 0.00	8.49 ± 0.12	95 ± 9	9.59 ± 0.06	8.75 ± 0.11	8.74 ± 0.08	73 ± 10	9.42 ± 0.05	8.77 ± 0.11	8.50 ± 0.09	63 ± 6	9.59 ± 0.06	8.68 ± 0.21	8.21 ± 0.12	96 ± 10
F85L	—	9.18 ± 0.06	7.93 ± 0.04	26 ± 3	9.09 ^a	7.68 ± 0.36	7.72 ± 0.14	10 ± 1	—	<6.5	<6.5	<6.5	—	8.10 ± 0.11	<6.5	<6.5
L104F	9.78 ± 0.17	—	8.08 ± 0.12	46 ± 5	9.50 ± 0.06	—	8.22 ± 0.07	27 ± 5	8.99 ± 0.06	—	7.25 ± 0.11	18 ± 2	9.35 ± 0.06	—	7.26 ± 0.10	37 ± 6
F85L/L104F	—	9.36 ± 0.18	8.02 ± 0.06	31 ± 5	9.80 ^a	8.40 ± 0.19	7.91 ± 0.09	7 ± 4	—	8.37 ± 0.06	7.35 ± 0.17	43 ± 28	9.88 ^a	8.01 ± 0.25	<6.5	<6.5
Y89S	9.31 ^a	9.29 ^a	8.18 ± 0.13	40 ± 4	9.63 ± 0.25	8.62 ^a	8.11 ± 0.16	19 ± 6	9.56 ^a	—	8.53 ± 0.13	33 ± 3	—	—	7.01 ± 0.23	32 ± 5
F85L/Y89S	NM	9.28 ± 0.30	8.02 ± 0.10	41 ± 8	NM	7.16 ± 0.04	<6.5	—	NM	7.86 ± 0.10	<6.5	<6.5	NM	7.93 ± 0.09	<6.5	<6.5
Y89S/L104F	NM	—	7.65 ± 0.04	7 ± 3	NM	NM	<6.5	—	NM	NM	<6.5	<6.5	NM	NM	<6.5	<6.5
Y108A	9.92 ± 0.09	—	8.30 ± 0.06	53 ± 2	9.78 ± 0.08	—	8.45 ± 0.24	40 ± 4	9.39 ± 0.13	—	7.93 ± 0.07	30 ± 2	8.73 ± 0.16	—	<6.5	<6.5
F109H	9.55 ^a	—	8.99 ± 0.10	95 ± 16	9.89 ± 0.04	—	9.01 ± 0.11	84 ± 25	9.67 ^a	—	8.83 ± 0.12	78 ± 15	9.74 ^a	—	8.03 ± 0.12	83 ± 26
F112Y	—	—	8.26 ± 0.10	32 ± 5	9.76 ± 0.05	—	8.39 ± 0.05	18 ± 3	—	—	8.15 ± 0.23	20 ± 5	—	—	7.36 ± 0.09	25 ± 3
F109H/F112Y	—	—	9.00 ± 0.14	80 ± 6	9.91 ± 0.08	—	8.94 ± 0.07	60 ± 2	—	—	8.97 ± 0.09	62 ± 4	—	—	7.67 ± 0.11	54 ± 4
L104F/F109H/ F112Y	9.82 ± 0.07	—	8.62 ± 0.13	67 ± 7	9.69 ± 0.13	—	8.35 ± 0.10	38 ± 3	9.75 ± 0.13	—	7.88 ± 0.02	38 ± 3	9.75 ± 0.28	—	<6.5	<6.5

^a For practical reasons, some binding experiments yielding wild-type-like results both in the preliminary tests and dose-response curves were not further investigated; these values are given for illustration purposes.

“Experimental Procedures”). The energies of interaction of Phe-85 and Trp-86 with the multiple C-H hydrogens of Leu-104 are −2.4 and −2.6 kcal/mol, respectively.

Structural and Functional Role of Aromatic Residues in TM3

Residues Phe-109 and Phe-112 are located in TM3 within the outer third of the membrane and are predicted to face toward the center of the helix bundle, as inferred from the molecular model of CCR5 (see above) or the rhodopsin template itself. The F109H mutation had little effect on the receptor function. Both the binding properties and the functional response of the mutant were closely similar to those of wt-CCR5 for all four ligands (Table I, Figs. 3 and 4). In contrast, the conservative F112Y substitution influenced strongly the activation of the receptor by its agonists. The potencies of RANTES, MIP-1α, and MIP-1β were relatively preserved, whereas that of MCP-2 was decreased by ~1 log. The efficacies of all ligands were however severely affected, with E_{max} values ranging from 10 to 25% of the ATP response (Table I). Remarkably, combining these two substitutions in the F109H/F112Y mutant significantly restored the functional response of the receptor, with E_{max} values ranging from 54 to 90% of the maximal cell response and improved of potencies for all four ligands. The L104F/F109H/F112Y change, which combine the three mutations of TM3, produced a receptor phenotypically close to that of the single L104F. Although binding affinities were wt-like, activation was affected differentially for the different agonists; RANTES was almost not affected, MCP-2 severely impaired, with MIP-1α and MIP-1β showing intermediate behaviors. This suggest an addition of effects of the L104F single mutant (significantly affected) and the F109H/F112Y double mutant (mild effect). This is not surprising considering that these motifs are located in distant part of the structure, as, in our model, Leu-104 interacts with TM2, whereas Phe-109 and Phe-112 face TM5 and TM6, respectively (see “Discussion”).

Mutant Y108^{3,32}A

Considering the selective effect on receptor function observed after mutation of transmembrane residues in TM2 and TM3, it appeared also interesting to test the putative role of residue Tyr-108. This locus, referred as position 3.32 in the generalized numbering scheme of Ballesteros (see “Experimental Procedures”), is known as an important binding site in a wide variety of GPCRs (reviewed in Refs. 6, 12, and 24). Site-directed mutagenesis has been used to demonstrate its central role in different receptors for neurotransmitters and peptides. The Y108A mutant was well recognized at the cell surface by antibodies targeting the N terminus of the receptor (mean fluorescence above 60% of signal for wt-CCR5), whereas fluorescence was significantly decreased for antibodies recognizing either the second loop or a combination of extracellular domains, possibly underlying a conformational modification of the extracellular loops of the receptor. This mutant exhibited a rather wild-type behavior following stimulation by RANTES, MIP-1β, or MIP-1α, with slightly reduced efficacies, but was completely unreactive to MCP-2. We could, however, measure high affinity binding of this ligand by competition binding assay (Fig. 3 and Table I). As for several other mutants described above, this mutant became unresponsive to MCP-2 without affecting the affinity for this ligand, whereas other CCR5 agonists (e.g. RANTES) were still able to stimulate it. It is known that GPCRs, including CCR5 (40), can adopt multiple active states that trigger different intracellular cascades and are differentially stabilized by various agonists. In this line, one could hypothesize that MCP-2 would not be able to induce Ca²⁺ increase

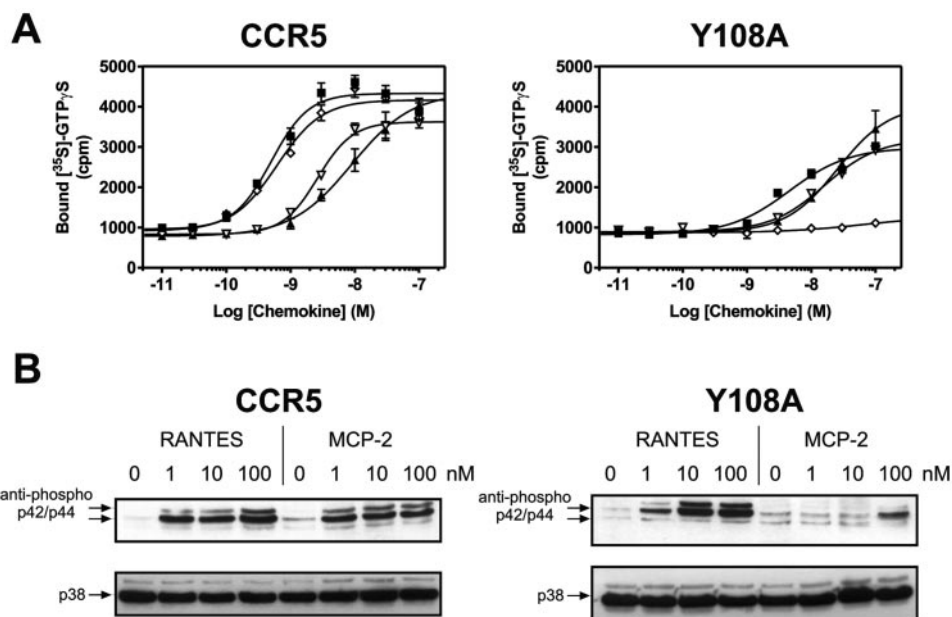


FIG. 5. **GTP γ S binding and MAP kinase activation assays of wt-CCR5 and the Y108A mutant.** A, functional response to RANTES (■), MIP-1 β (▲), MIP-1 α (▼), and MCP-2 (◇) of CHO-K1 cells expressing wt-CCR5 and the Y108A mutant in the GTP γ S assay (see “Experimental Procedures”). Data are presented as raw counts/min, and all points were run in triplicate (*error bars*: S.E.). The displayed curves represent a typical experiment out of at least two performed independently. B, immunoblot detection of activated p42/p44 MAP kinase revealed with anti-phospho-p42/p44. CHO-K1 cells expressing either the wt-CCR5 or the Y108A mutant were stimulated with RANTES or MCP-2 at three different concentrations (1, 10, and 100 nM). Detection of p38 by Western blotting was used to control that an equal amount of material was loaded in each lane. A typical experiment of three performed independently is shown.

through this mutant receptor, while being able to trigger other intracellular cascades. As shown in Fig. 5A, the four natural agonists could trigger GTP γ S binding through the wt receptor. In this assay, RANTES was the most potent agonist, whereas MCP-2 appeared more potent than MIP-1 α and MIP-1 β . As observed with the aequorin assay, MCP-2 was unable to stimulate the Y108A mutant in the GTP γ S assay. It has been shown that chemokine-induced activation of CCR5 can lead to activation of p42/p44 (44, 45). As shown in Fig. 5B, stimulation of CCR5 by RANTES or MCP-2 led to the dose-dependant phosphorylation of p42/p44 MAP kinases. In this assay, RANTES stimulated the Y108A mutant, although with a reduced efficiency as compared with wt-CCR5, and MCP-2 was almost inactive, except for a weak response observed at 100 nM.

The specific alteration of the mutant response to MCP-2 is reminiscent of the behavior observed in our previous study, in which mutations of the TXP motif also affected preferentially the biological response to MCP-2, without significantly affecting the binding of this chemokine. In the wt model, the Tyr-108 side chain is positioned in the face-to-edge orientation (T-shaped) with the indole ring of Trp-86 (see Fig. 7A). This type of π - σ aromatic-aromatic interaction has been described as stabilizing a protein structure (46). It is expected that the conformational changes induced in TM2 by mutations affecting the TXP motif would relocate the side chain of Trp-86, located four residues apart, and as a consequence affect its interaction with Tyr-108.

DISCUSSION

The three-dimensional model of CCR5 based on the rhodopsin crystal structure (including the specific modeling of the TM2-TM3 interface as described above; Fig. 6) provides a coherent framework to interpret the mutagenesis data detailed under “Results.” We propose that the residues varying between CCR5 and CCR2 at the level of the TM2-TM3 aromatic cluster are forming a specific interaction motif. In the wt receptor, Phe-85^{2,59} would interact with Leu-104^{3,28}, whereas Tyr-89^{2,63}

would H-bond with Thr-99^{3,23}, and we suggest that the substitutions observed in the CCR2 sequence are indeed correlated. It is important to note that this modeled TM2-TM3 interface provides a hydrophobic environment for Thr-82^{2,56} of the TXP motif in TM2, essentially through the side chain of Leu-104 (Fig. 7A). Thus, Thr-82 orients the C γ atom toward this hydrophobic environment, and the O γ atom toward the polar peptide bond of the backbone. The additional hydrogen bond between the O γ atom of Thr-82 and the carbonyl group increases the magnitude of the Pro-kink and this TXP motif is a structural determinant involved in chemokine-induced activation (13).

To analyze in this structural framework the consequences of the amino acid substitutions explored experimentally, several of the mutations were introduced in our model, and we specifically studied the structural and dynamical properties of the extracellular part of the TM2-TM3 interface using MD simulations (see “Experimental Procedures”). This modeling procedure allows to propose a description of the TM interface for the mutants and suggests the nature of the structural changes that might lead to alterations of the receptor function (Fig. 7).

Structural Interpretation of Mutations Located at the Extracellular End of TM2 and TM3—The F85L mutation weakens the interaction between the side chain of this TM2 residue and Leu-103 and Leu-104 in TM3, as a Leu-Leu interaction is not of the same magnitude as a Leu-Phe interaction. As a consequence, in the simulation, Leu-85 side chain reorients away from TM3 (Fig. 7B).

Replacing Leu-104 by Phe dramatically modifies the TM2-TM3 interface. The aromatic side chain of Phe-104 would optimally interact with the other aromatic side chains in a face to edge configuration (46). Thus, in the molecular dynamic simulations, the side chain of Phe-104 tends to achieve this interaction with the aromatic side chains of both Phe-85 and Trp-86 (Fig. 7C). However, the side chain of Phe-104 in this conformation is bulkier than that of Leu, resulting in a significant reorientation of Phe-85 side chain toward the periphery of the

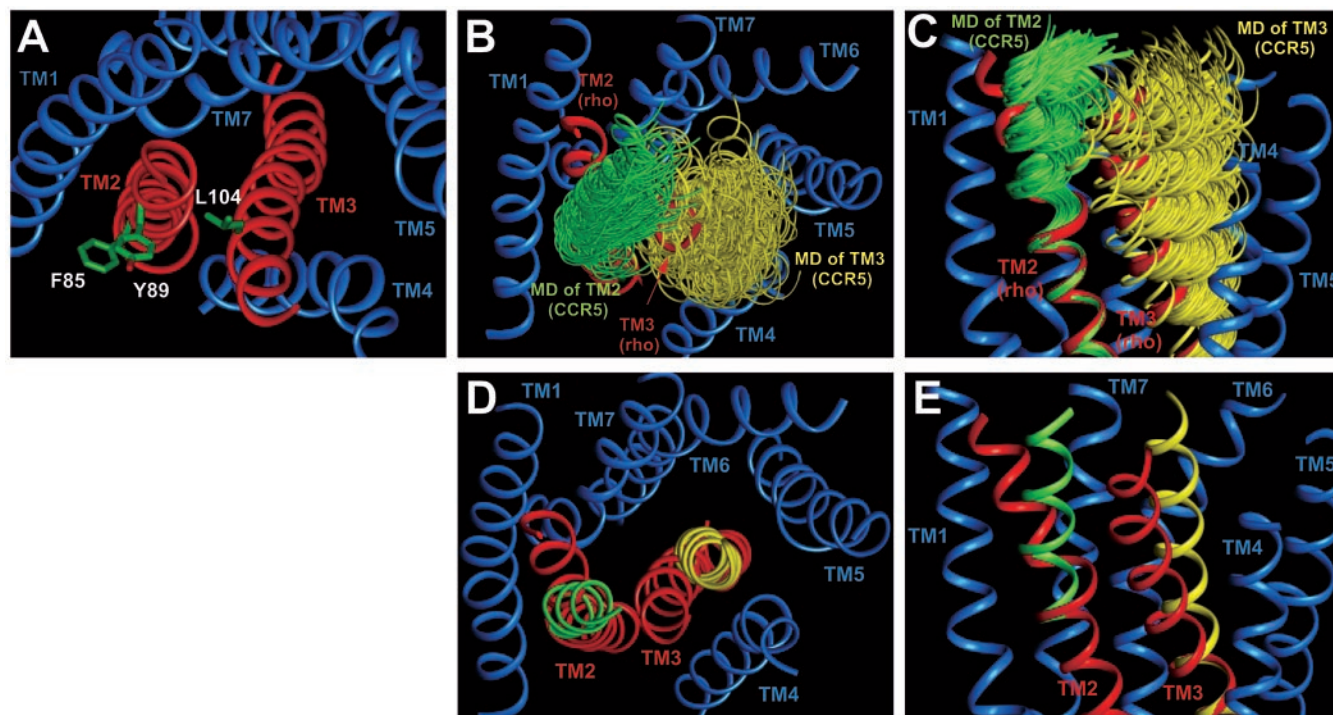


FIG. 6. Modeling procedure of the TM2-TM3 interface. *A*, side-chain positions of residues 85, 89, and 104 in a model of the transmembrane domain of CCR5 based rigorously on the rhodopsin template. The C_{α} trace is shown as *ribbon*, in *red* for TM2 and TM3, in *blue* for the other helices. In such a model, these side chains face the membrane, which is hardly compatible with the functional role suggested by the mutagenesis experiments. *B*, superimposition of 100 structures from independent Molecular Dynamics simulations of TM2 (in *green*) and TM3 (in *yellow*) onto the rhodopsin template (see “Experimental Procedures” for details). Only the C_{α} trace is shown for each structure, represented as *ribbon*. Viewed from the extracellular side. *C*, same as the previous panel but viewed from the side. It appears clearly that the conformational spaces are almost not overlapping. In particular, the conformational space of TM3 moves away from that of rhodopsin, allowing room for the kinked TM2 of CCR5. *D* and *E*, extracellular and side views of the representative structures of TM2 (in *green*) and TM3 (in *yellow*) selected from the simulations and used to construct the interface.

TM bundle, and in a weakening of the TM2-TM3 interface. It is important to note that the L104F mutation increases the polarity of the Thr-82 side chain environment. Thus, the presence of the electron-rich clouds of Phe-104 aromatic ring might facilitate hydrogen bonding to the O_{γ} atom of Thr-82, in a manner similar to that proposed for hydrogen bonding between benzene and water (47). This would contrast with the wild-type receptor, in which a hydrogen bond is formed with the polar peptide bond of the backbone. As already discussed, the additional hydrogen bond of the Thr to the peptide bond has a significant influence on the conformation of the helix (13, 26).

In the double F85L/L104F mutant, the aromatic side chain of Phe-104 is now located between Leu-85 and Leu-103 (Fig. 7D). Thus, the electron-rich clouds of the aromatic ring interact with the electron-poor C-H hydrogens of both Leu-85 and Leu-104. Notably, this mode of interaction of Phe-104 places Leu-85 in the proximity of Thr-82, mimicking the hydrophobic environment of Thr-82 in the wild-type receptor (see above). Moreover, the aromatic side chain of Tyr-89 is interacting in a face to edge configuration with Phe-104. Thus, it appears from this simulation that the F85L/L104F mutant would partly restore the packing of the TM2-TM3 interface.

This could explain the improvement in cell-surface expression and binding affinity for MIP-1 α and MIP-1 β , between the F85L and F85L/L104F mutants (see Table I). As the conformation of the short ECL1 (four residues) is likely influenced by the packing of the TM2-TM3 interface, we would suggest that point mutations (like F85L) could modify the conformation of the EC domain and affect the binding of ligands.

The triple mutant F85L/L104F/Y89S is intriguing. Intuitively, one would expect that, having replaced all differing aromatic positions into the CCR2 corresponding residues, the

resulting mutant would show a better functional phenotype than the single or double mutant (being closer to the functional CCR2 receptor). However, it appeared that this triple mutant is not expressed at the cell surface (see Fig. 2), suggesting severe misfolding of the protein. Our modeling suggests that the addition of the Y89S substitution to the double F85L/L104F mutant would strongly modify the TM2-TM3 interface, because the shorter and non-aromatic side chain of Ser-89 cannot fulfill the interaction with both Thr-99 and Phe-104 (Fig. 7D). We hypothesize that this major structural difference between this mutant interface and the wt structure could be a factor responsible for the weak expression, either through a perturbation of the folding process, or through destabilization of the folded protein, leading to rapid internalization and/or degradation. In the single Y89S mutant, this modification of the packing of TM2 and TM3 would not happen as the Phe-85-Leu-104 interaction maintains a proper distance between the two helices. Moreover, Thr-99^{2,23} would tend to interact with the side chain of Gln-93^{2,67} (Fig. 7C), changing moderately the interface. Notably, the Y89S mutant shows a normal level of expression and is moderately affected in the functional tests, suggesting that the Tyr-89-Thr-99 interaction proposed here is necessary for full functional efficiency, but not for the structural stability of the receptor. The double mutants F85L/Y89S and Y89S/L104F show a level of expression reduced by ~50%, a functional response strongly affected for F85L/Y89S and almost completely abolished for Y89S/L104F, underlining the increase in structural perturbation caused by the additional mutations.

Combining the experimental results with our modeling approach leads to the following picture; the function of the CCR5 receptor is strongly dependent on the interface between the extracellular ends of TM2 and TM3, which is determined by a

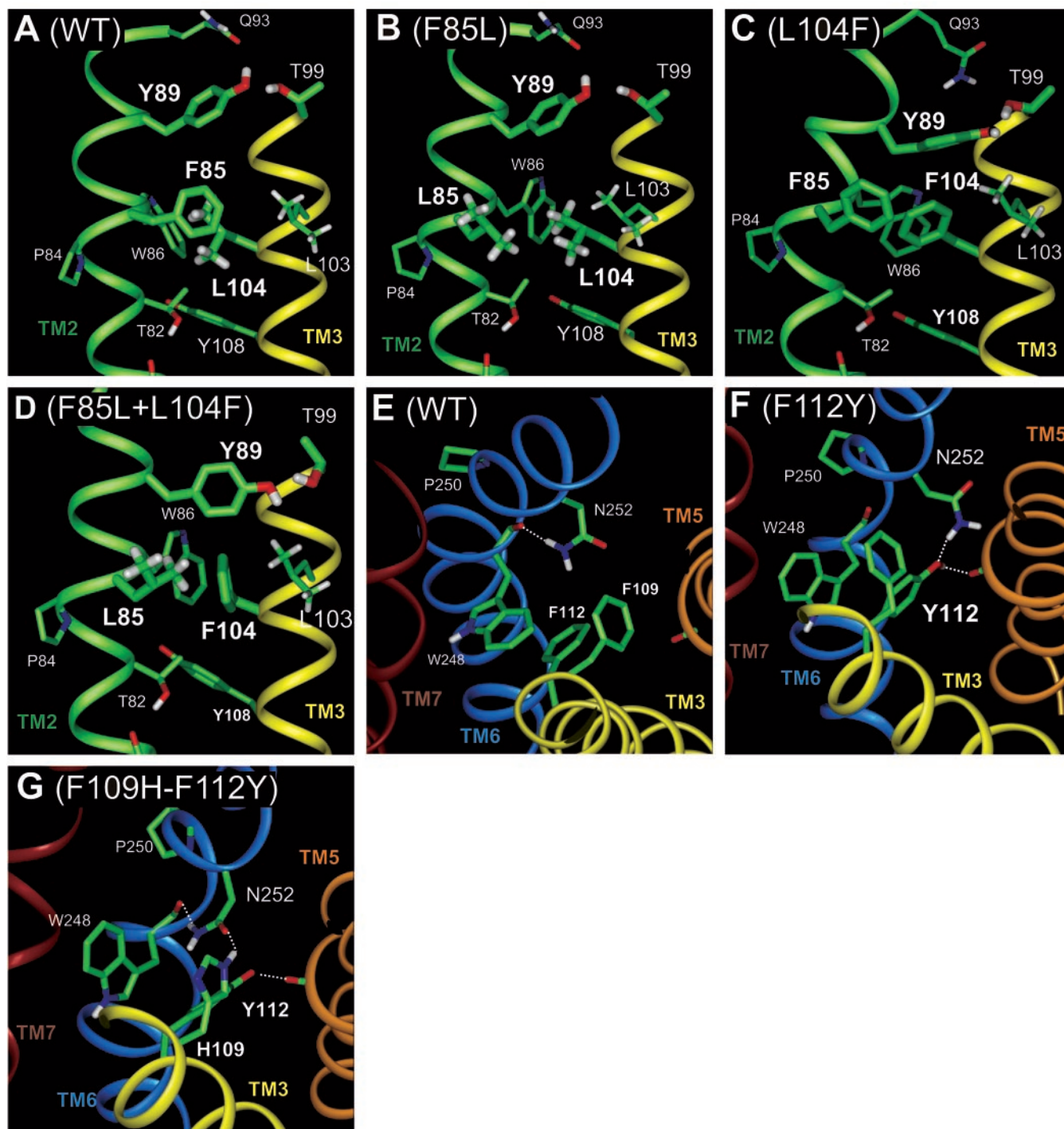


FIG. 7. Molecular models of TM2-TM3 interface and the TM3-TM6 interaction for wt and mutant receptors. *A*, model of the TM2-TM3 interface obtained for the wt receptor. Only interacting side chains are shown, highlighting the proposed Phe-85-Leu-104 and Tyr-89-Thr-99 interactions (see text for details). *Panel B* and *C* show the models for F85L and L104F mutants, respectively, illustrating the loss of interaction at the 85–104 locus for these receptors. *D*, model of the double F85L/L104F mutant showing the proposed recovered interaction. *E*, wt model showing the location of Phe-109 and Phe-112 and featuring the conformation of Asn-252 interacting with the backbone in TM6. *F*, model of the F112Y mutant, showing how this mutant could modify the conformation of Asn-252 in TM6. *G*, model of the double F109H/F112Y, illustrating how the F109H additional mutation would recover the structural effect of the F112Y mutant.

series of interhelical interactions. The structural and dynamical properties of this interface are maintained by, at least, two polar interactions: Tyr-89-Thr-99 and Phe-85-Leu-104. These interactions are in equilibrium with each other, providing balanced structural constraints. Perturbing this interface by mutating one of these residues would modify this equilibrium and affect the function of the receptor.

This model implies that, in the case of the CCR2 receptor, the

TM2-TM3 interface is organized differently, and that the substitutions tested here are counterbalanced by other changes in the sequence. In particular, one can spot the T99^{3,23}A change between the two receptors (see Fig. 1), but other changes (like A92^{2,66}N or Q93^{2,67}E) could also be important. Interestingly, a chimeric construct involving ICL1, TM2, ECL1, and TM3 of CCR2 in a CCR5 background appeared to be well expressed and functional (35), suggesting that interactions between TM2

and TM3 are sufficient to obtain structural stability and functionality (as the other helices were strictly from CCR5).

The Extracellular Ends of TM2 and TM3 Are Involved in the Activation Mechanism—By mutating the Thr-2.56-X-Pro-2.58 motif, we previously have shown that the structural integrity of TM2 is crucial for CCR5 function (13). According to the nature of the substitution (various residues in place of Thr-82^{2.56}, or Ala instead of Pro-84^{2.58}), we could modulate the extent of the structural perturbation, which was translated into a functional defect. However, the different agonists of CCR5 were affected differently by these mutations, suggesting that this part of the receptor is involved in the activation process in a ligand-specific manner.

We proposed that this TXP motif governs the structural and dynamical properties of the extracellular end of TM2. By looking at the specific role of Phe-85^{2.59} and Tyr-89^{2.63}, we now probe the elements involved in the ligand-induced activation in this particular part of the TM bundle. Interestingly, we find the same trend as that observed after mutating the TXP motif; the ligand sensitivity to the mutations is variable, RANTES being the least affected agonist, whereas MCP-2 is the most sensitive.

Structural Modeling of Mutants Involving the Middle of TM3—Phe-109 and Phe-112, variable between CCR5 and CCR2, are not facing TM2 in the CCR5 model, but are oriented toward TM5 and TM6. We therefore undertook full bundle MD simulation to model (see “Experimental Procedures”) the possible effects of the F109^{3.33}H, F112^{3.36}Y, and F109H/F112Y mutations, and the putative interaction between these residues and TM5 and/or TM6.

Although the F109H change does not modify the pattern of helix-helix interactions as compared with the wt receptor (data not shown), changing Phe-112 for Tyr modifies the interactions between TM3 and TM6 (Fig. 7, panels E and F). In our simulation, the hydroxyl group added by the mutation forms a H-bond with Asn-252^{6.52} in TM6. In the wt receptor, this Asn H-bonds back to the backbone carbonyl of Trp-248^{6.48}, and also interacts through its H_{δ1} atom with the aromatic ring of Phe-112 (Fig. 7E). Pointing inside the bundle, residue Asn-252^{6.52} is highly conserved among CC-chemokine receptors, and position 6.52 is known to be functionally important in several rhodopsin-like GPCRs (6). In particular, this position is involved in ligand binding, ligand selectivity, or receptor activation in a significant number of peptide (48–52) and neurotransmitter (16, 17, 53) receptors, suggesting a possible functional role of the corresponding residue in chemokine receptors as well. In addition, the H-bond proposed here to form with the backbone could also be important. The conserved Pro, present in TM6 of most rhodopsin-like receptors (Pro-6.50) is known to be crucial for their function, most probably through the structural action of the proline. It has been proposed that, in the context of an α -helix, polar residues H-bonding the backbone in the vicinity of a Pro could significantly modulate the structure of the proline-induced deformation, and therefore be functionally relevant (13, 54). Interestingly, in the F112Y mutant, the polar interaction between Tyr-112^{3.36} and Asn-252^{6.52} changes the conformation of the asparagine away from the backbone, hence preventing it from H-bonding with the backbone carbonyl of Trp-248^{6.48}.

Therefore, the polar interaction between Tyr-112 and Asn-252 could strongly modify the functional properties of Asn-252 by interfering with its putative interaction with the ligand and/or its structural role. It is important to note that, in contrast to the mutations located in the TM2-TM3 interface, the F112Y mutation affects all four agonists in a similar manner. The activation profile is qualitatively similar to that of the wt

receptor (the potency order is preserved), but the potency and efficacy of agonists are reduced \sim 3-fold.

As detailed under “Results,” the double F109H/F112Y mutant exhibits a behavior similar to that of the wt receptor, hence showing that adding the F109H mutation restores the function lost in the F112Y mutant. Although such functional recovery may suggest a direct interaction between the two residues, this is very unlikely in the context of an α -helix, in which a His and a Tyr cannot interact together when separated by three positions. In our model, the F109H substitution modifies *indirectly* the effect of the F112Y mutation (Fig. 7G). Although Tyr-112 now interacts with the backbone carbonyl of Gly-202^{5.46}, His-109 interacts with Asn-252, leading to a reorientation of the side chain that mimics the wt situation, including a recovery of the H-bond between Asn-252^{6.52} and the carbonyl of Trp-248^{6.48}. The effect of the single F112Y mutation is therefore counterbalanced by the addition of the histidine, which allows the reorientation of Asn-252^{6.52}, leading to an almost normal behavior of this putative functional motif.

Conclusions—The wealth of structural, biophysical, and biochemical data accumulated during the last years provides valuable insights into the activation mechanism of GPCRs. It is well established that the activation process requires helix motions; in particular, movements of TM3, TM6, and TM7 have been evidenced (5, 6). The importance of the TM2-TM3 interface in the activation of CCR5 support the concept that other parts of the TM bundle are also involved in this mechanism. As suggested previously (13), we hypothesize that the active role of the TM2-TM3 interface in the activation process is somehow specific to chemokine receptors, as suggested by the conservation of the TXP motif in TM2, and of the aromatic cluster in the extracellular ends of TM2 and TM3. Although our work suggests that TM2 (and possibly TM3) would actually move upon chemokine-induced activation, biophysical approaches would be necessary to demonstrate the motion of these helices during activation.

Acknowledgments—Expert technical assistance was provided by M. J. Simons. We thank Mathias Mack for kindly providing monoclonal antibodies and Juan Ballesteros for inspiring discussions.

REFERENCES

1. Baggiolini, M. (1998) *Nature* **392**, 565–568
2. Gerard, C., and Rollins, B. J. (2001) *Nat. Immunol.* **2**, 108–115
3. Berger, E. A., Murphy, P. M., and Farber, J. M. (1999) *Annu. Rev. Immunol.* **17**, 657–700
4. Blanpain, C., Migeotte, I., Lee, B., Vakili, J., Doranz, B. J., Govaerts, C., Vassart, G., Doms, R. W., and Parmentier, M. (1999) *Blood* **94**, 1899–1905
5. Meng, E. C., and Bourne, H. R. (2001) *Trends Pharmacol. Sci.* **22**, 587–593
6. Gether, U. (2000) *Endocr. Rev.* **21**, 90–113
7. Farrens, D. L., Altenbach, C., Yang, K., Hubbell, W. L., and Khorana, H. G. (1996) *Science* **274**, 768–770
8. Dunham, T. D., and Farrens, D. L. (1999) *J. Biol. Chem.* **274**, 1683–1690
9. Gether, U., Lin, S., Ghanouni, P., Ballesteros, J. A., Weinstein, H., and Kobilka, B. K. (1997) *EMBO J.* **16**, 6737–6747
10. Marjamaki, A., Frang, H., Pihlavisto, M., Hoffren, A. M., Salminen, T., Johnson, M. S., Kallio, J., Javitch, J. A., and Scheinin, M. (1999) *J. Biol. Chem.* **274**, 21867–21872
11. Abdulaev, N. G., and Ridge, K. D. (1998) *Proc. Natl. Acad. Sci. U. S. A.* **95**, 12854–12859
12. Ji, T. H., Grossmann, M., and Ji, I. (1998) *J. Biol. Chem.* **273**, 17299–17302
13. Govaerts, C., Blanpain, C., Deupi, X., Ballet, S., Ballesteros, J. A., Wodak, S. J., Vassart, G., Pardo, L., and Parmentier, M. (2001) *J. Biol. Chem.* **276**, 13217–13225
14. Wess, J., Gdula, D., and Brann, M. R. (1991) *EMBO J.* **10**, 3729–3734
15. Fong, T. M., Cascieri, M. A., Yu, H., Bansal, A., Swain, C., and Strader, C. D. (1993) *Nature* **362**, 350–353
16. Kim, J., Wess, J., van Rhee, A. M., Schoneberg, T., and Jacobson, K. A. (1995) *J. Biol. Chem.* **270**, 13987–13997
17. Cho, W., Taylor, L. P., Mansour, A., and Akil, H. (1995) *J. Neurochem.* **65**, 2105–2115
18. Lee, S. Y., Zhu, S. Z., and el Fakahany, E. E. (1996) *Recept. Signal. Transduct.* **6**, 43–52
19. Roth, B. L., Shoham, M., Choudhary, M. S., and Khan, N. (1997) *Mol. Pharmacol.* **52**, 259–266
20. Javitch, J. A., Ballesteros, J. A., Weinstein, H., and Chen, J. (1998) *Biochemistry* **37**, 998–1006
21. Colson, A. O., Perlman, J. H., Jinsi-Parimoo, A., Nussenzveig, D. R., Osman,

- R., and Gershengorn, M. C. (1998) *Mol. Pharmacol.* **54**, 968–978
22. Rhee, M. H., Nevo, I., Bayewitch, M. L., Zagory, O., and Vogel, Z. (2000) *J. Neurochem.* **75**, 2485–2491
23. Simpson, M. M., Ballesteros, J. A., Chiappa, V., Chen, J., Suehiro, M., Hartman, D. S., Godel, T., Snyder, L. A., Sakmar, T. P., and Javitch, J. A. (1999) *Mol. Pharmacol.* **56**, 1116–1126
24. Ballesteros, J. A., and Weinstein, H. (1995) *Methods Neurosci.* **25**, 366–428
25. Lopez-Rodriguez, M. L., Vicente, B., Deupi, X., Barrondo, S., Olivella, M., Morcillo, M. J., Behamu, B., Ballesteros, J. A., Salles, J., and Pardo, L. (2002) *Mol. Pharmacol.* **62**, 15–21
26. Ballesteros, J., Deupi, X., Olivella, M., Haaksma E., and Pardo, L. (2000) *Biophys. J.* **79**, 2754–2760
27. Palczewski, K., Kumasaka, T., Hori, T., Behnke, C. A., Motoshima, H., Fox, B. A., Le, T., I, Teller, D. C., Okada, T., Stenkamp, R. E., Yamamoto, M., and Miyano, M. (2000) *Science* **289**, 739–745
28. Kelley, L. A., Gardner, S. P., and Sutcliffe, M. J. (1996) *Protein Eng.* **9**, 1063–1065
29. Bower, M. J., Cohen, F. E., and Dunbrack, R. L. (1997) *J. Mol. Biol.* **267**, 1268–1282
30. Tsuzuki, S., Honda, K., Uchimar, T., Mikami, M., and Tanabe, K. (2000) *J. Am. Chem. Soc.* **122**, 3746–3753
31. Olivella, M., Deupi, X., Govaerts, C., and Pardo, L. (2002) *Biophys. J.* **82**, 3207–3213
32. Darden, T., York, D., and Pedersen, L. (1993) *J. Chem. Phys.* **98**, 10089–10092
33. Case, D. A., Pearlman, D. A., Caldwell, J. W., Cheatham, T. E., Ross, W. S., Simmerling, C. L., Darden, T. A., Merz, K. M., Stanton, R. V., Cheng, A. L., Vincent, J., Crowley, M., Ferguson, D. M., Radmer, R. J., Seibel, G. L., Singh, U. C., Weiner, P. K., and Kollman, P. A. (1997) *AMBER5*, University of California, San Francisco
34. Cornell, W. D., Cieplak, P., Bayly, C. I., Gould, I. R., Merz, K. M., Jr., F., D. M. Spellmeyer, D. C., Fox, T., Caldwell, J. W., and Kollman, P. A. (1995) *J. Am. Chem. Soc.* **117**, 5179–5197
35. Samson, M., LaRosa, G., Libert, F., Paindavoine, P., Dethoux, M., Vassart, G., and Parmentier, M. (1997) *J. Biol. Chem.* **272**, 24934–24941
36. Rizzuto, R., Pinton, P., Carrington, W., Fay, F. S., Fogarty, K. E., Lifshitz, L. M., Tuft, R. A., and Pozzan, T. (1998) *Science* **280**, 1763–1766
37. Stables, J., Green, A., Marshall, F., Fraser, N., Knight, E., Sautel, M., Milligan, G., Lee, M., and Rees, S. (1997) *Anal. Biochem.* **252**, 115–126
38. Blanpain, C., Lee, B., Vakili, J., Doranz, B. J., Govaerts, C., Migeotte, I., Sharron, M., Dupriez, V., Vassart, G., Doms, R. W., and Parmentier, M. (1999) *J. Biol. Chem.* **274**, 18902–18908
39. Blanpain, C., Wittamer, V., Vanderwinden, J. M., Boom, A., Renneboog, B., Lee, B., Le Poul, E., El Asmar, L., Govaerts, C., Vassart, G., Doms, R. W., and Parmentier, M. (2001) *J. Biol. Chem.* **276**, 23795–23804
40. Blanpain, C., Vanderwinden, J. M., Cihak, J., Wittamer, V., Le Poul, E., Issafras, H., Stangassinger, M., Vassart, G., Marullo, S., Schlindorff, D., Parmentier, M., and Mack, M. (2002) *Mol. Biol. Cell* **13**, 723–737
41. Schagger, H., and von Jagow, G. (1987) *Anal. Biochem.* **166**, 368–379
42. Lee, B., Sharron, M., Blanpain, C., Doranz, B. J., Vakili, J., Setoh, P., Berg, E., Liu, G., Guy, H. R., Durell, S. R., Parmentier, M., Chang, C. N., Price, K., Tsang, M., and Doms, R. W. (1999) *J. Biol. Chem.* **274**, 9617–9626
43. Steiner, T., and Koellner, G. (2001) *J. Mol. Biol.* **305**, 535–557
44. Dairaghi, D. J., Franz-Bacon, K., Callas, E., Cupp, J., Schall, T. J., Tamraz, S. A., Boehme, S. A., Taylor, N., and Bacon, K. B. (1998) *Blood* **91**, 2905–2913
45. Misse, D., Esteve, P. O., Renneboog, B., Vidal, M., Cerutti, M., St Pierre, Y., Yssel, H., Parmentier, M., and Veas, F. (2001) *Blood* **98**, 541–547
46. Burley, S. K., and Petsko, G. A. (1985) *Science* **229**, 23–28
47. Suzuki, S., Green, P. G., Bumgarner, R. E., Dasgupta, S., Goddard, W. A., III, and Blake, G. A. (1992) *Science* **257**, 942–945
48. Zoffmann, S., Gether, U., and Schwartz, T. W. (1993) *FEBS Lett.* **336**, 506–510
49. Fong, T. M., Yu, H., Cascieri, M. A., Underwood, D., Swain, C. J., and Strader, C. D. (1994) *J. Biol. Chem.* **269**, 2728–2732
50. Kask, K., Berthold, M., Kahl, U., Nordvall, G., and Bartfai, T. (1996) *EMBO J.* **15**, 236–244
51. Turner, C. A., Cooper, S., and Pulakat, L. (1999) *Biochem. Biophys. Res. Commun.* **257**, 704–707
52. Huang, X. P., Nagy, P. I., Williams, F. E., Peseckis, S. M., and Messer, W. S., Jr. (1999) *Br. J. Pharmacol.* **126**, 735–745
53. Granas, C., Nordvall, G., and Larhammar, D. (1998) *J. Recept. Signal. Transduct. Res.* **18**, 225–241
54. Ri, Y., Ballesteros, J. A., Abrams, C. K., Oh, S., Verselis, V. K., Weinstein, H., and Bargiello, T. A. (1999) *Biophys. J.* **76**, 2887–2898